TECHNICAL MEMORANDUM

596

The MACC Global Fire Assimilation System: First Emission Products (GFASv0)

J.W. Kaiser, J. Flemming, M.G. Schultz[1], M. Suttie and M.J. Wooster[2]

Research Department

[1]Forschungszentrum Jülich (FZJ), Germany
[2]King's College London (KCL), United Kingdom

August 20, 2009

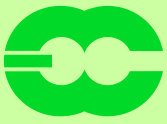

European Centre for Medium-Range Weather Forecasts
Europäisches Zentrum für mittelfristige Wettervorhersage
Centre européen pour les prévisions météorologiques à moyen terme

Series: ECMWF Technical Memoranda

A full list of ECMWF Publications can be found on our web site under:
http://www.ecmwf.int/publications/

Contact: library@ecmwf.int

European Centre for Medium-Range Weather Forecasts
Shinfield Park, Reading, RG2 9AX, England

Abstract

The D-FIRE sub-project of MACC is producing real time fire emissions with a Global Fire Assimilation System (GFAS). The emissions will be used by the regional and global forecast production systems in MACC. The first version of the fire emission products, GFASv0, is based on the GEMS fire emission product but is scaled such that it reproduces the global annual emission budget of the GFEDv2 inventory. Preliminary comparisons of modelled smoke plumes with other systems' smoke plumes indicates that the GFASv0 products are applicable for fire plume forecasting. They are released with a previously agreed interface that consists of archiving in the MARS database of regular latitude-longitude emission fields for several species with 0.1 deg spatial resolution and 1 hour temporal resolution. The release enables the MACC partners to implement and technically test the interface. Furthermore, the fire emissions may already be used in the MACC forecasting systems after testing their effect on the particular system's forecasting skill. Feedback on the product interface as well as its performance in forecasting applications is encouraged.

1 Introduction

Emissions from biomass burning constitute an important boundary condition for the modelling of the atmospheric composition. On a global scale, they contribute significantly to budgets of several species like CO and organic matter. Their contribution to the carbon cycle is of a similar size as the combined contributions of fossil fuel burning in Europe and in North America. On a regional scale, large fire events can dominate the surface air quality.

The most accurate way of monitoring global fire emissions is based on satellite observations of the actual fires because they vary strongly on all timescales from hours to decades. Several available satellite observations need to be merged in a Global Fire Assimilation System (GFAS) to obtain fire emission estimates with global coverage at high temporal resolution. The global and regional forecasting systems of the future GMES Atmospheric Core Service (GACS) need such fire emission estimates in real time. The GEMS project has consequently started the implementation of a GFAS. It currently delivers global daily fields of observed Fire Radiative Power (FRP) based on the observations of SEVIRI on-board the geostationary Meteosat-8/9 satellites and MODIS on-board the polar orbiting Terra and Aqua satellites.

The D-FIRE sub-project of MACC develops the GFAS further. As a first step global fire emission fields for a comprehensive list of species are derived from observed FRP fields. They are based on the observed daily FRP product of the GEMS system. The emission fields are made available to all MACC partners in a suitable data format and in real time in the so-called "GFASv0" product. They will also be made publicly available on the MACC data server. This memo describes GFASv0. Even though the product is not properly validated yet, there are indications that it may be more suitable for real time forecasting purposes than retrospective inventories.

GFASv0 is released to enable the implementation of the technical interface in the MACC forecasting systems, scientific testing of the emissions in these systems and, possibly, use in the MACC forecasts. Any feedback is encouraged and will be addressed in future updates.

Section 2.1 motivates the use of FRP observations as opposed to hot spot ones. The scientific method for fire emission estimation is described in Sections 2.2–2.3. A number of properties, like budgets, of the emissions in GFASv0 are shown and compared to GFEDv2 in Section 2.4. The technical setup of the data processing chain is outlined in Section 3. Section 4 and Appendix A contain essential instructions for accessing and using GFASv0, and Section 5 outlines the plans for future upgrades.

2 Scientific Description

2.1 Why FRP?

Traditionally, fire emissions are calculated as a fraction ("emission factor") of the burnt biomass, which is in turn calculated as a fraction ("combustion efficiency") of the available fuel load [adapted from Seiler and Crutzen, 1980]. However, the fuel load estimation is related to the identification of the relevant biome and constitutes the key uncertainty in existing fire emission monitoring systems [Reid et al., 2009]. Recently, Wooster et al. [2003] and Ichoku et al. [2005] have shown that this error source can be avoided by determining the biomass combustion rate directly from observations of the fire radiative power (FRP). The underlying assumption is that the same fraction of the released chemical energy is converted to thermal radiation in fires of all types. Since this assumption is thought to be more accurate than the assumptions involved in calculating available fuel load, the GFASv0 estimates are based on FRP observations.

2.2 Method

2.2.1 Global Field of Fire Radiative Power

Global fields of observed FRP are derived following Kaiser et al. [2009b]. The approach uses FRP datasets of the SEVIRI and MODIS instruments as input and consists of two steps:

1. The fire datasets of MODIS and SEVIRI express FRP in Watts for each pixel i: $FRP(i)$. The satellite data have 1 km and 3 km spatial resolution at sub-satellite point, respectively. Each pixel i of a dataset k can be classified as either observed fire ($FRP_k(i) > 0$), observed non-fire ($FRP_k(i) = 0$), or not observed, most notably due to cloud cover. Each individual satellite dataset is represented by two global fields:

   - For each global grid cell j, the FRP density $\rho_k(j)$ [W m^{-2}] is calculated by normalising the sum of the observed $FRP_k(i)$ with the total observed pixel area $A_k(i)$:

   $$\rho_k(j) = c_k \times \frac{\sum_i FRP_k(i)}{\sum_i A_k(i)} \qquad (i \in \text{grid cell } j,\ FRP_k(i) \geq 0 \text{ observed}) \tag{1}$$

   Fire concealment by cloud cover is intrinsically corrected by including the observations with $FRP_k(i) = 0$. This approach assumes that the fire distribution within a grid cell does not depend on the cloud cover.[1] The correction factor c_k is used to remove biases in different FRP datasets k. We use MODIS as standard and adjust the SEVIRI data following the finding that SEVIRI underestimates FRP by 40–50% on a regional-scale when compared to MODIS [Roberts and Wooster, 2008]:

   $$c_k = \begin{cases} 1 & (k \text{ is MODIS data}) \\ 2 & (k \text{ is SEVIRI data}) \end{cases} \tag{2}$$

   - For each grid cell j, the total observed area

   $$a_k(j) = \sum_i A_k(i) \qquad (i \in \text{grid cell } j,\ FRP_k(i) \geq 0 \text{ observed}) \tag{3}$$

   is stored as a quantitative measure for the accuracy of calculated the FRP density ρ.

[1] Currently, the same correction is automatically applied for the water-covered part of the grid cell. This needs to be corrected in a future version.

2. The two polar orbiting MODIS instruments deliver a fire product every 5 minutes along their orbit track. Coverage is global and they take on average around 6 hours to deliver a new fire product of a previously viewed area. The geostationary SEVIRI instrument delivers fire products covering the same area every 15 minutes, but it only covers a fixed Earth disk (Europe, South and North Africa, and part of South America in four separate datasets). Let the index k distinguish all these different datasets and t_k denote their respective observation times. The spatially merged and temporally averaged observed FRP density for the temporal window $[t_1, t_2]$ is then calculated as

$$\rho = \frac{\sum_k a_k \times \rho_k}{\sum_k a_k} \qquad (k:\ t_k \in [t_1, t_2]) \tag{4}$$

and, again, the total observed area provides a quantitative measure of the accuracy:

$$a = \sum_k a_k \qquad (k:\ t_k \in [t_1, t_2]) \tag{5}$$

In both steps, the observed areas A_k, a_k and a are interpreted statistically as the inverses of the variances of the corresponding FRP and FRP density fields FRP_k and ρ_k and ρ.

An indicative fire observation return period T can be calculated from the fraction of the grid cell observed during the temporal window $[t_1, t_2]$:

$$T = \frac{g}{a} \times (t_2 - t_1) \tag{6}$$

where g denotes the area of the grid cells. Crucially for this calculation, Equation 5 implies that $a > g$ occurs in well-observed regions. The observation return period T is an illustrative characterisation of the observation system, see Figure 2, but it is not directly used in the emission flux computation.

2.2.2 *Conversion of Fire Radiative Power to Species Emissions*

The fire emission flux density f_s [kg s^{-1} m^{-2}] of any species s is approximately proportional to the FRP. It is therefore calculated as

$$f_s = \rho \times \alpha \times \beta_s \quad , \tag{7}$$

where the units of α are kg J^{-1}, $\rho \times \alpha$ is the combustion rate density [kg(dry matter) s^{-1} m^{-2}], and β_s are biome-dependent emission factors [kg(species s) kg^{-1}(dry matter)].

We use emission factors β_s from the GFEDv2 inventory [van der Werf et al., 2006, Andreae and Merlet, 2001], which distinguish between the three land cover classes "savanna", "tropical forest" and "other forest". The geographical land cover map is derived from the MODIS land cover classification.

Based on measurements of experimental fire, Wooster et al. [2005] have found $\alpha = 0.368 \cdot 10^{-6}$ kg(biomass) J^{-1} $\approx$ $0.245 \cdot 10^{-6}$ kg(dry matter) J^{-1}, where a factor of 1.5 is assumed to convert mass of dry matter to biomass. However, such a value results in a severe underestimation of emissions, see Section 2.4.4. Therefore, the GFAS emission fluxes are normalised to GFEDv2 fluxes: With $\alpha = 1.37 \cdot 10^{-6}$ kg(dry matter) J^{-1}, the average of the GFASv0 fluxes of black carbon, sulfur dioxide, carbon monoxide, carbon dioxide and methane during the time period 1 Oct 2008–17 Jun 2009 equals the average of the corresponding monthly fluxes in GFEDv2 during the years 2000–2007.

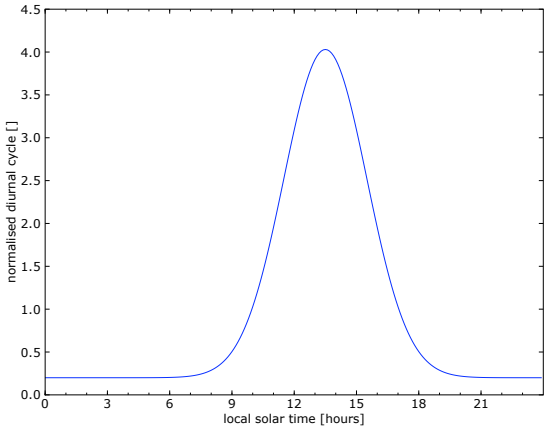

Figure 1: Assumed diurnal cycle $p(t_l)$. [unitless]

2.3 Diurnal Cycle

In order to provide a first order approximation for the strong diurnal variation of biomass burning, an artificial diurnal cycle p is superimposed on the daily observed emission fields f_s. The diurnal cycle is described as the sum of a constant and a Gaussian function that peaks in early afternoon, cf. Figure 1:

$$p(t_l) = w + (1-w)\,\frac{24\text{h}}{\sigma\sqrt{2\pi}}\exp\left(-\frac{1}{2}\left(\frac{t_l - t_0}{\sigma}\right)^2\right) \tag{8}$$

$$\text{with} \quad w = 0.2 \tag{9}$$

$$t_0 = 13.5\text{h} \tag{10}$$

$$\sigma = 2\text{h} \quad , \tag{11}$$

where t_l denotes the local solar time. The chosen weight w implies that 90% of the emissions occur during daytime and 10% during nighttime.

The choice of parameters is an ad-hoc compromise between the typical diurnal cycles observed in the tropics and the continental US by Giglio [2007] and Zhang and Kondragunta [2008], respectively: The former typically display a burning peak between 13 and 16 hours local solar time and virtually vanishing nighttime emissions in many regions (Brazilian cropland and Northern being the exceptions with significant nighttime emissions). The latter find a peak fire activity between 10 and 15 hours local solar time and attribute 50–85% (except for shrublands fires in 2005) of the burnt area to this time period.

The next version of GFAS is planned to make use of the temporal resolution of the observations instead of prescribing a fixed diurnal cycle.

2.4 Results

2.4.1 Observational Coverage and Daily FRP Fields

An example of an observed daily FRP density field, along with the corresponding observation return periods is reproduced in Figure 2, top plot. Early February lies towards the end of the sub-Saharan fire season, which is still dominating the global picture. The lower two plots show indicative return periods T for the two MODIS instruments and SEVIRI, respectively. The high sampling frequency of SEVIRI is evident while the two MODIS instruments achieve almost global coverage during one day. They do not produce fire data for regions with snow or ice cover, though.

All fire observations are affected by cloud cover, which persistently limits fire observability in the ITCZ, e.g. in Central Africa and, on this day, Libya and Southern Algeria. In grid cells without any observation, the daily observed FRP density ρ is set to zero. This introduces a negative bias in the data, but the only possible remedy would be to use burnt area observations retrospectively. In grid cells with only few observations (large T), ρ is obviously relatively inaccurate. However, the error is expected to be random noise without bias.

2.4.2 Time-resolved Emission Fields

Snapshots of CO emission fields at four different times of 12 July 2009 are shown in Figure 3. The daytime peak of the artificial diurnal cycle $p(t_l)$ manifests itself in particularly large emissions in Alaska at 0 UTC, in South-East Asia at 6 UTC, in Africa at 12 UTC and in South America at 18 UTC. The nighttime contribution leads to a similar outline of the areas with any fire emissions throughout the 24-hour period.

2.4.3 Emission Budgets

The seasonal emission patterns of the GFASv0 emissions are shown in Figure 4, where only the data from the available time series covering 1 October 2008 to 12 July 2009 is used. The logarithmic colour scale reveals that fires occur throughout the year in many regions. However, the strong seasonal cycles are also evident with very distinctive fire activity in the different seasons: (season labels refer to the Northern hemisphere)

autumn: South America

winter: Sub-Saharan Africa

spring: peninsular Asia

summer: Southern Africa, Siberia and Alaska.

Several global monthly budgets of GFASv0 emissions from Oct 2008 to June 2009 are shown in Figure 5, left plot, along with the corresponding global budgets of GFEDv2 averaged over the years 2000 to 2007. The GFASv0 time series for different species compare similarly to GFEDv2. However, small differences between the time series of sulphur dioxide and black carbon arise from the geographical variations of the emission factors.

The linear scale in the right plot of Figure 5 makes the differences between the global GFASv0 and GFEDv2 emissions of carbon monoxide more discernible. There are believed to be three main reasons for the differences between GFASv0 and GFEDv2.

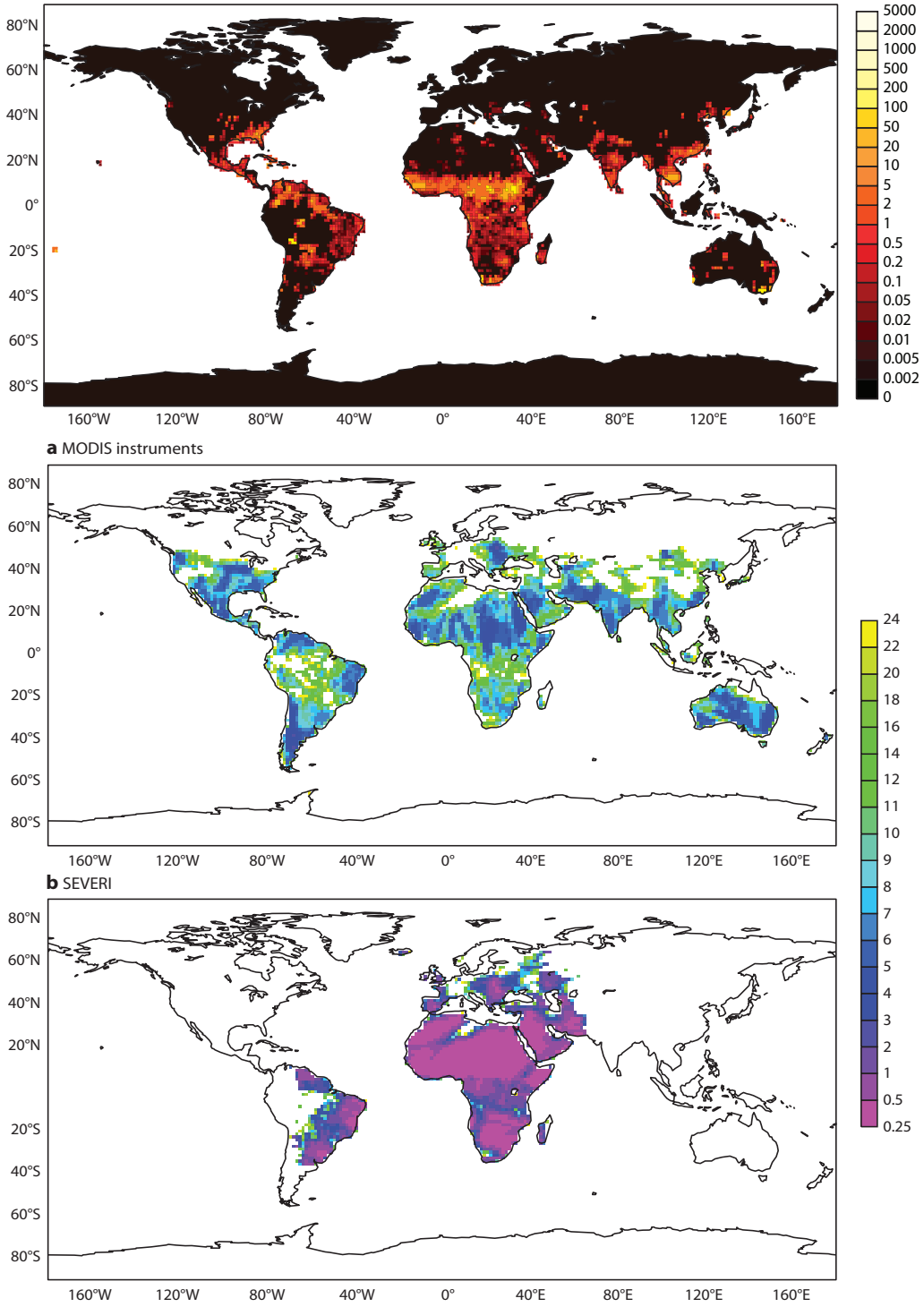

Figure 2: Observed FRP density ρ [mW m^{-2}, T159 resolution] (top) and indicative return periods T [hours] of the MODIS and SEVIRI fire observations (middle, bottom) on 7 Feb 2009. [Kaiser et al., 2009a]

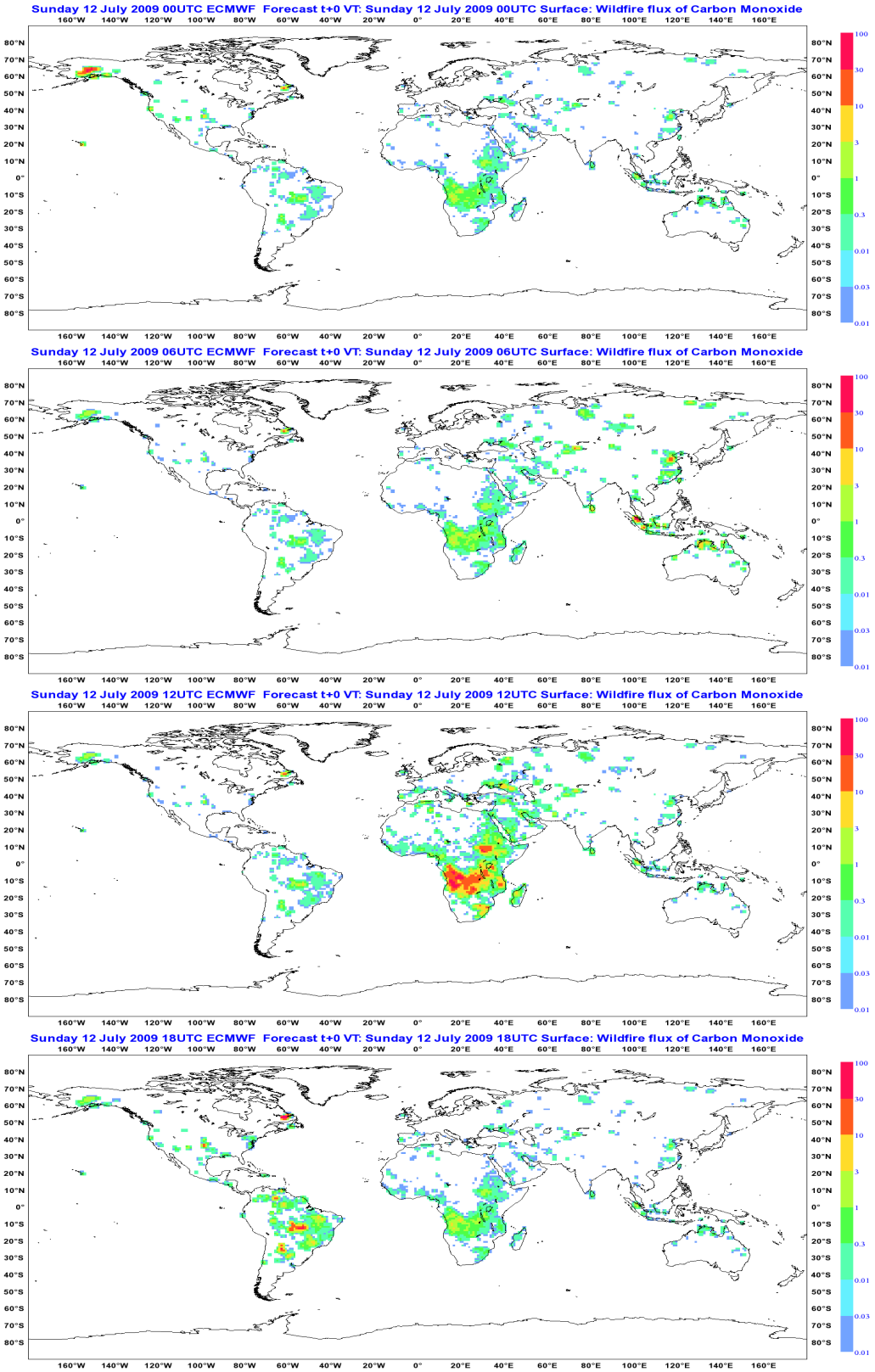

Figure 3: GFASv0 diurnally resolved fire emission density of CO [kg h^{-1} km^{-2}] on 12 July 2009: 00–01, 06–07, 12–13, 18–19 UTC (top to bottom).

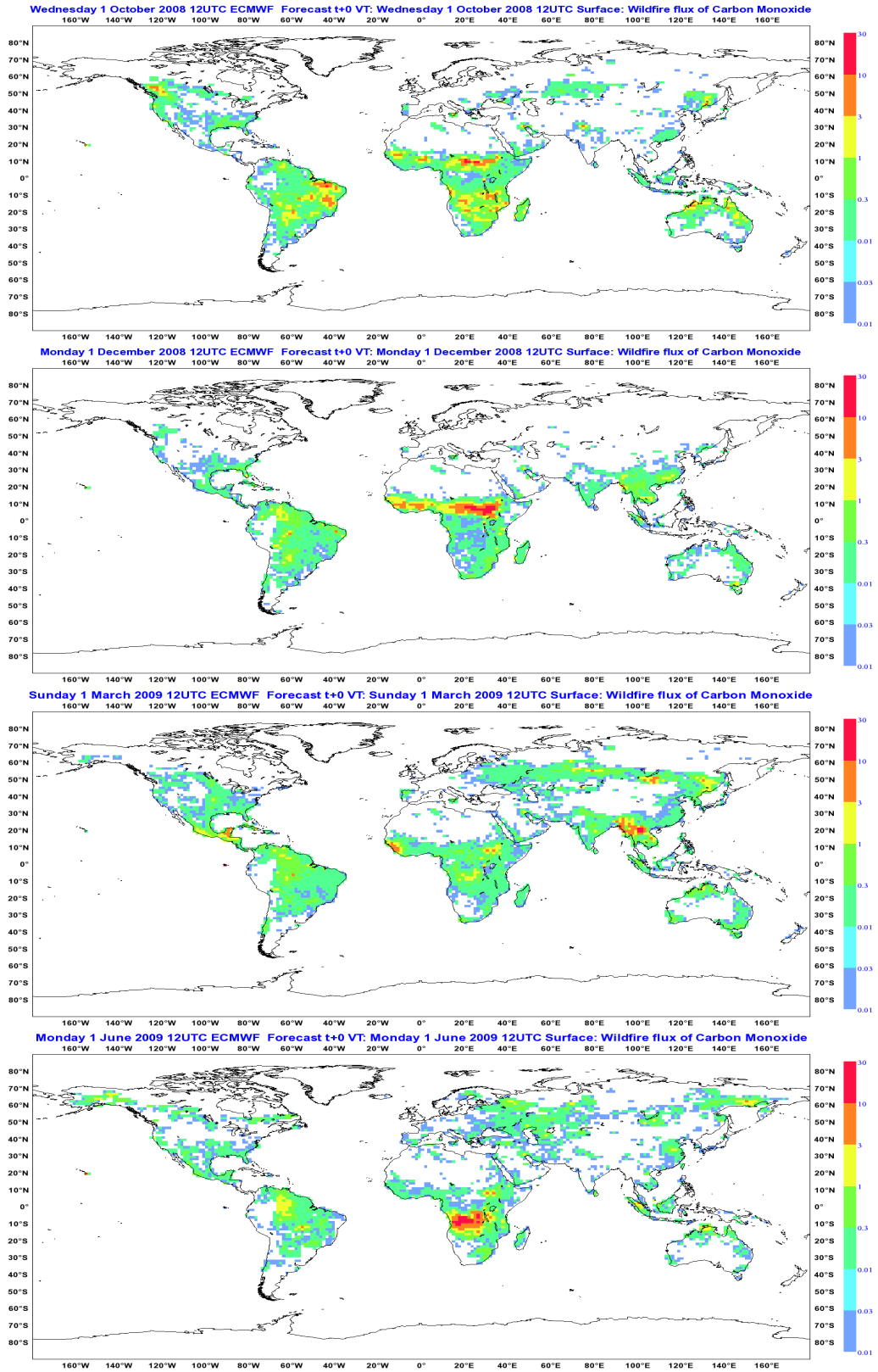

Figure 4: GFASv0 time series of CO fire emissions [g month^{-1} m^{-2}] by season: ON, DJF, MAM, JJ (top to bottom) for 1 Oct 2008–12 Jul 2009.

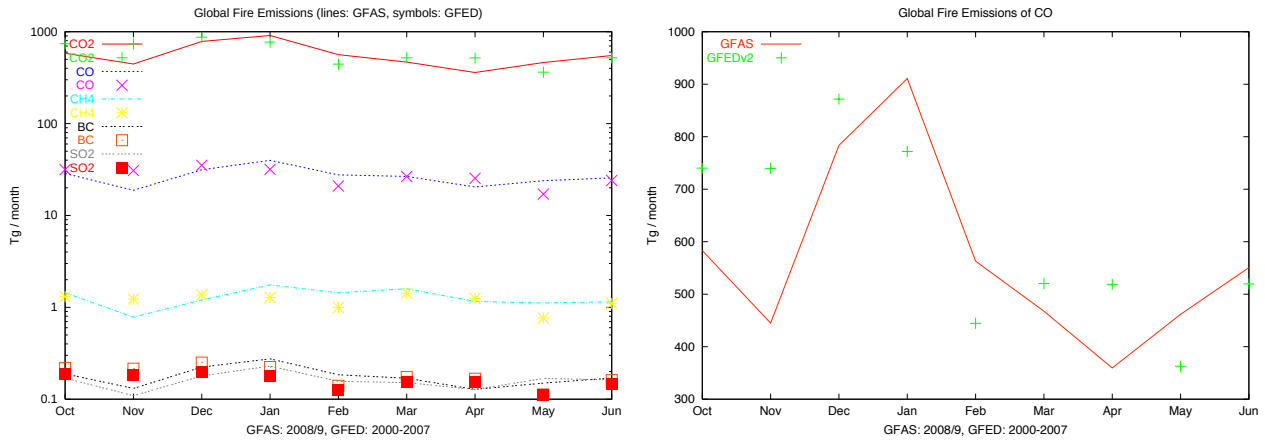

Figure 5: GFASv0 and GFEDv2 time series of monthly global fire emissions of several species (left, logarithmic y-axis) and CO (right, linear y-axis): GFASv0 for 1 Oct 2008–17 Jun 2009, GFEDv2 for the corresponding monthly averages of 2000–2007.

- Inter-annual variations, since different time periods are compared.
- Algorithms with different core assumptions for the calculations.
- Inaccuracy of minor assumptions in GFASv0, e.g. an ad-hoc bias removal for SEVIRI FRP observations.

The geographic contributions to the differences are shown in Figure 6. GFASv0 has annual cycles that are qualitatively consistent with those of GFEDv2. The variations in y-axes scaling reveal that the global fire emission budget in the investigated time period is dominated by the Northern Africa fire season, and consequently also the determination of the scaling factor α, see section 2.2.2.

The GFASv0 emissions in Northern Hemisphere Africa and Europe (NHAE), Southern Hemisphere Africa (SHAf) and Southern Hemisphere America (SHAm) are dominated by the SEVIRI observations. During the periods with little fire activity GFASv0 seems to be biased low in all three regions. This may be caused by the relatively high detection threshold of the SEVIRI fire observations, which results in it missing a high percentage of fires during periods with smaller fires. The fact that the bias is largest in SHAm indicates that SEVIRI misses particularly many fires near the edge of its observational disk, which is unsurprising due to the very large pixel areas present at these extreme viewing angles. Attributing the apparent temporal shift in the NHAE fire emissions would require further studies.

The GFASv0 emissions in Northern Hemisphere America (NHAm), Northern Hemisphere Asia (NHAs) and Southern Hemisphere Asia and Australia (SHAA) are entirely calculated from the MODIS FRP data. Thus they are based on the same MODIS observations and the same emission factors as GFEDv2. The main difference is that GFEDv2 is based on the MODIS hot spot data and consequently employs a different methodology for calculating the biomass combustion rate. Discrepancies may also arise from the sampling of different time periods. The annual cycles of GFASv0 and GFEDv2 generally agree well. NHAm displays a strong low bias of GFASv0 during the period with low fire intensity. It resembles the behaviour in SHAf and SHAm even though no SEVIRI observations are used and may partially originate from inter-annual variability.

It is common for regional fire emission estimates from different inventories and monitoring systems to display inconsistencies of several hundred percent. In this context, the GFAS emissions may be of acceptable accuracy for forecasting applications, even though there is a clear potential for improvements.

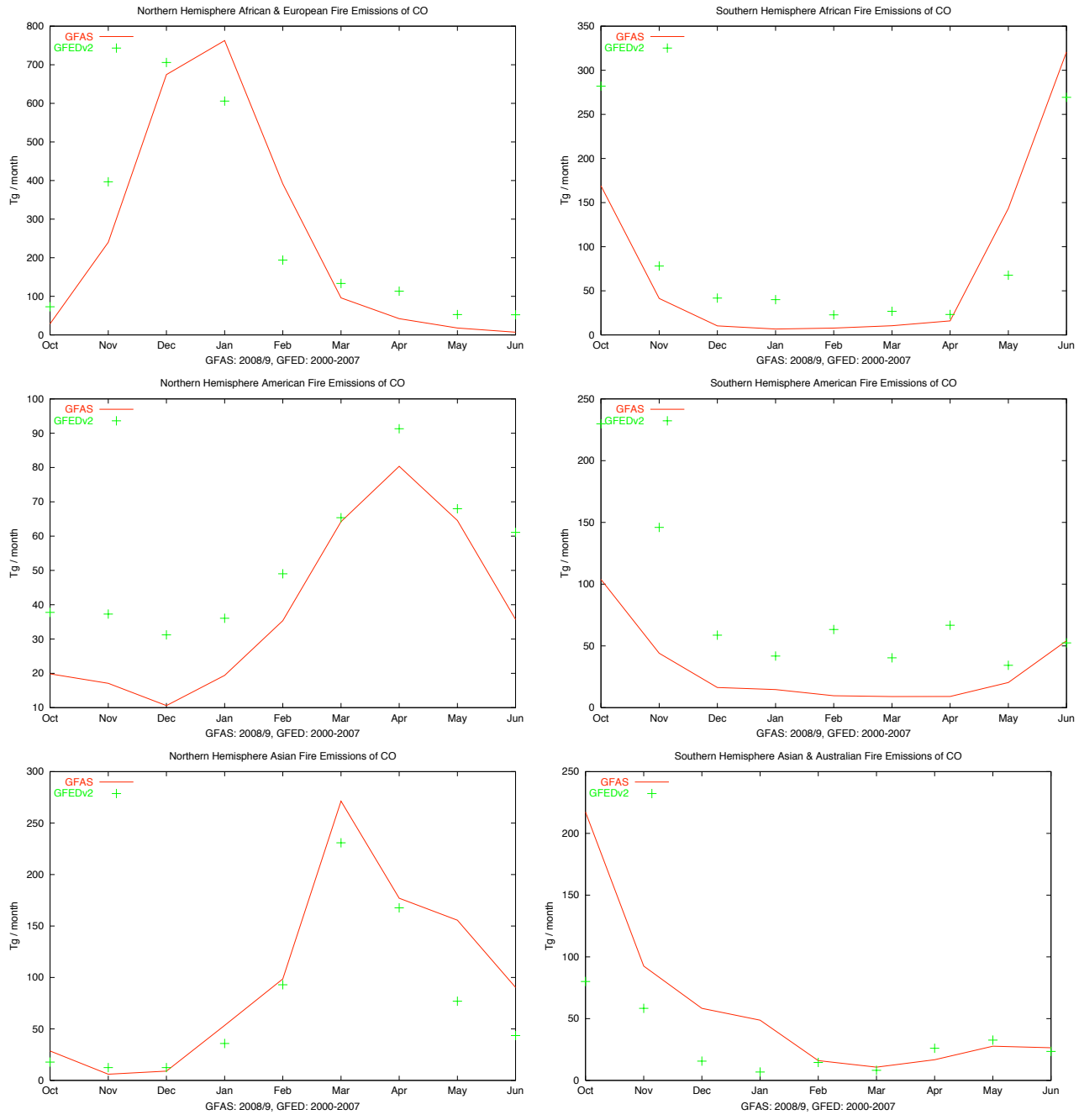

Figure 6: GFASv0 and GFEDv2 time series of monthly fire emissions of CO in several regions: GFASv0 for 1 Oct 2008–17 Jun 2009, GFEDv2 for the corresponding monthly averages of 2000–2007.

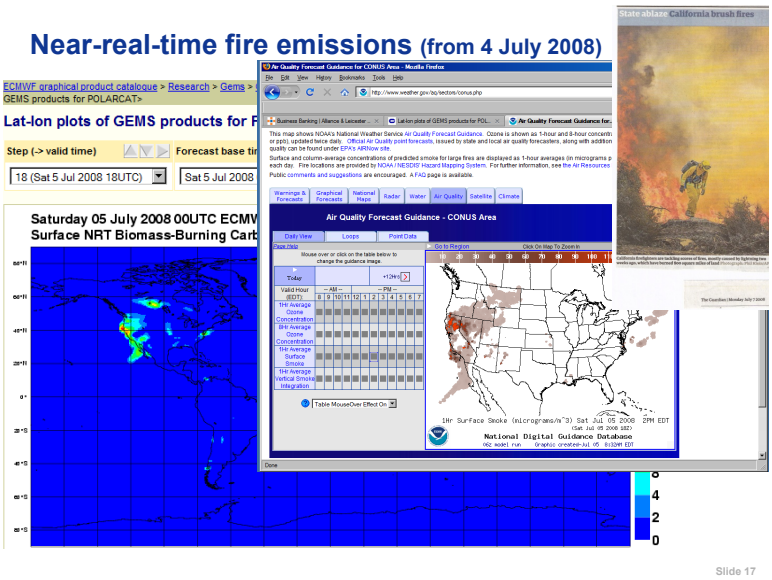

Figure 7: Comparison of GEMS carbon monoxide plume and NOAA-generated smoke plume forecasts for fires in California in July 2008. [from presentation by A. Simmons at GEMS Final Assembly, Jülich, April 2009.]

2.4.4 Test Forecast of Atmospheric Carbon Monoxide

The GEMS GRG sub-project has used an earlier version of the GFAS emissions for global real time forecasts of pyrogenic CO plumes since 3 July 2008. These emissions used the scaling value $\alpha = 0.368 \cdot 10^{-6}$ kg(dry matter) J^{-1} and consequently were about four times smaller than the GFASv0 emissions. Both have the same geographical and temporal patterns, though. The forecast plume concentrations of CO were subsequently confirmed to be too low. However, limited qualitative comparisons of the forecast plume shapes with other plume modelling systems show reasonable agreement: Figure 7 compares the forecasts by GEMS and NOAA of plumes from Californian fires just two days after GEMS GRG started its plume forecasts. Figure 8 compares arctic fire plumes predicted by GEMS and FLEXPART on 5 and 23 July 2008. While the GEMS system is clearly in its spin-up phase on 5 July, the patterns on 23 July bear extensive resemblance. This confirms the validity of geographical patterns and the day-to-day variations of the GFASv0 emissions. Therefore, they may already be more suitable for forecasting applications than retrospective fire emission inventories like GFEDv2.

3 Implementation

3.1 Satellite Data Access

The FRPPIXEL dataset from SEVIRI observations is generated in real time by the EUMETSAT LandSAF in Portugal. The dataset is separated into four regions: Europe, North Africa, South Africa and South America. It consists of two hdf5 files for each region and every 15 minute time slot. A detailed description can be found in the "Product User Manual" that is available on the LandSAF web site `http://landsaf.meteo.pt`.

A Linux PC cron job updates a local rolling archive of the FRPPIXEL product every hour from `ftp://safmil.meteo.pt/Products/FRPPIXEL/`. The products are also retrieved from EUMETCast and archived in ECFS at `ec:/oparch/gems/seviri_frp/YYYYMM/DD/`, where `YYYY`, `MM` and `DD` denote year, month and day of the observation. Future versions of GFAS are expected to rely solely on EUMETCast.

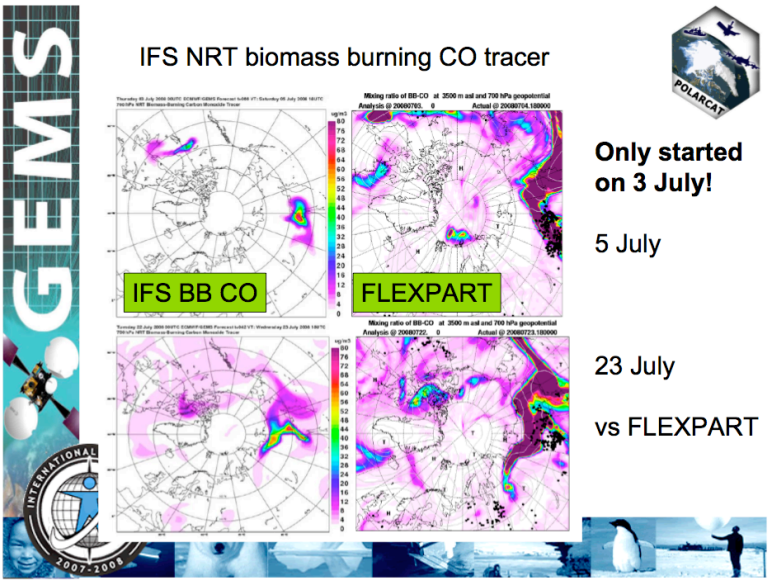

Figure 8: Comparison of GEMS carbon monoxide plume and NOAA-generated smoke plume forecasts for fires in California in July 2008. [from presentation by K. Law at GEMS Final Assembly, Jülich, April 2009.]

FRP is also part of the MODIS MOD14 data. Additional geolocation information is extracted from the MOD03 data. Collection 5 MODIS data are used. They are download from NOAA at `ftp://nanuk.eosdis.nasa.gov:/pub/am1/MODIS/MOD14/MOD14.AYYYYDDD.HHMM.hdf.gz` for Terra, and `ftp://nanuk.eosdis.nasa.gov:/pub/pm1/MODIS/MOD14/MOD14.PYYYYDDD.HHMM.hdf.gz` for Aqua, where `YYYY` is the year, `DDD` is day of year, and `HHMM` is the UTC time of the start of the granule. The data are archived in ECFS at `ec:/oparch/gems/modisfire/col5_nrt/aqua[terra]/YYYYMM/DD/MOD14.P[A]YYYYDOY.*.hdf.gz` and `ec:/oparch/gems/modisgeo/col5_nrt/aqua[terra]/YYYYMM/DD/MOD03.P[A]YYYYDOY.*.hdf.gz`. The data are also available in a rolling archive on disk on a high availability Hewlett-Packard cluster (`acq3`) to enable fast access by the necessary operational processing task in-house.

3.2 Satellite Data Preprocessing

The hourly cron job on the Linux PC converts each of the SEVIRI and MODIS datasets to global GRIB fields of FRP density ρ_k and total observed area a_k with the reduced Gaussian resolution T159, i.e. about 125 km. The fields are stored in a rolling archive on the Linux PC.

The conversion makes heavy usage of the ECMWF software GRIB API, see `http://ecmwf.int/products/data/software/grib_api.html`. It is, amongst others, used to assign the observation pixels to GRIB grid cells, which is is the computationally heaviest element of the entire processing chain.

3.3 Daily FRP Maps

A daily cron job on the Linux PC merges the gribified SEVIRI and MODIS data of the previous day to yield the daily observed FRP density field ρ, which is subsequently stored in ECFS at `ec:/GEMS/AER/FIRE/FRPv0/YYYY/MM/DD/`.

3.4 Emission Maps and Diurnal Cycle

The experiment `f7i1`, which is triggered daily on the ECMWF supercomputer `c1a`, converts the daily observed FRP density ρ data to emission fields for the different species, again in resolution T159, and archives them in the MARS database. The experiment `f7i2`, which is subsequently triggered, interpolates the emission onto a regular latitude-longitude grid with 0.1 deg resolution, applies the artificial diurnal cycle p, and archives the daily and hourly fields in MARS.

4 How to Use the Emission Fields

4.1 Data Access

The fire emission fields are stored in the MARS database, which is available on virtually all ECMWF computer systems, e.g. `ecgate` and `c1a`. They are identified by the experiment ID, currently `f7i2`. The different species are identified by their GRIB parameter IDs. Appendix A lists an example shell script for retrieving emission fields from MARS. The field's time stamps corresponds to the middle of their periods of validity: Daily fields are stored with a time stamp of 1200, hourly fields have time stamps of HH30, where HH denotes the hour. Currently, emissions are available for C, CO_2, CH_4, CO, SO_2, PM2.5, total particulate matter, organic carbon and black carbon.

The example script uses a proprietary program, firepolate090820, for flux-conserving interpolation to the required resolution. MACC project partners are welcome to use this program. All users can, of course, use their own flux-conserving interpolation software. For assistance, please contact `mailto:j.kaiser@ecmwf.int`.

The emission fields typically become available in MARS briefly before 0500 UTC on the day after their validity. We recommend to assume persistence of the diurnally resolved emissions as forecast for the next few days, until the release of fire emission forecasts by D-FIRE.

The GFASv0 product time series stretches back to 1 October 2008 to enable performance testing over an extended time interval.

4.2 Notification of Product Updates

All changes to the fire products will be announced on an email list. All users and interested parties are strongly advised to subscribe to this list by sending and email to `mailto:sympa@lists.ecmwf.int`, quoting "subscribe fire" in the subject. Please also state your affiliation and the nature of your interest in the products (1-2 sentences) in an email to `mailto:j.kaiser@ecmwf.int`. You can un-subscribe any time by sending an email to `mailto:sympa@lists.ecmwf.int`, quoting "unsubscribe fire" in the subject.

4.3 Caveats

Users of the GFASv0 product should bear the following limitations in mind:

- Custom grid resolution specifications must be avoided in the MARS retrieval because the implicit interpolation routines are not suitable for fire emission fields.

- The intrinsic resolutions of the products are still 1 day and about 125 km (T159).
- Observational gaps are not filled yet. Therefore, satellite data outages may lead to vanishing emissions in the affected regions. Such outages typically occur an a few days per year. Likewise, persistent cloud cover may inhibit fire observations and emissions in the some regions.
- The fire emission processing chain is not in a strictly operational mode yet. The first experience shows that availability at 0500 UTC is between 95% and 100%. Therefore, users with time-critical applications are advised to include a back-up solution, e.g. use of the fire emissions delivered one day earlier.

5 Outlook

D-FIRE will implement several improvements of its emission products over the course of the MACC project. All updated product versions will be archived with new experiment IDs, so that users can switch by just setting an experiment ID. The earlier versions will be discontinued after an appropriate transition period during which both products are available. It is important that users subscribe to the fire product email list to stay informed on any product updates, see section 4.2.

Forecasts of fire emissions covering several days will eventually be delivered in addition to emission analysis fields in real time. They will be archived in MARS in additional fields with parameter $step > 0$.

The GFED fire emission inventory will also be archived in MARS, so that users can switch to this inventory by choosing a different experiment ID in the MARS retrieval. For the inventory, the temporal and spatial resolution might be reduced to 1 day and 0.5 deg to prevent extreme multiple archiving of the same inventory fields. Additionally, a real time version of GFED will be made available under a dedicated experiment ID.

The fire emissions will also be made publicly available on the MACC data server.

A number of updates are foreseen that will improve the accuracy of the real time fire emissions without altering the user interface. They include:

- operational processing: The entire processing chain will be moved to high-availability computer systems at ECMWF.
- 0.1 deg spatial resolution throughout the processing chain
- dynamic determination of the diurnal cycle from the observations
- improved bias correction between the different satellite observations
- inclusion of additional satellite observations, in particular by the geostationary GOES satellites
- forecasting of the global fire activity with a statistical model
- filling of observation gaps with data assimilation into the model of global fire activity
- improve emission factors β_s and scaling factor α: They will be derived from comparisons of GFAS budgets with GFED budgets of the same time period and, eventually, from inversions of atmospheric plume analyses generated by the MACC systems.
- modify definition of weights A_k to

  - compensate for the so-called butterfly-effect of the MODIS scan geometry
  - reduce weights of SEVIRI observations near the edge of its observation disk
  - account for FRP accuracy estimates in satellite products
  - distinguish between satellite pixel foot print and sampling sizes
- include information from land-sea mask in coastal grid cells
- filter thermal observations that arise from other processes, e.g. gas flares and volcanoes.

Acknowledgements

Many people have contributed to the implementation of this product. We would like to thank Axel Bonet, Enrico Fucile, Manuel Fuentes, Sinisa Curic, Nils Wedi and Gianpaolo Balsamo for their help in setting up the processing chain. Collaboration with Gareth Roberts has pioneered our application of FRP data for emission estimation. EUMETSAT and its LandSAF were very helpful for making a suitable SEVIRI FRP product available. Guido van der Werf has provided the emission factors from GFED. Jean-Jacques Morcrette has provided the GEMS aerosol model for plume simulation tests. Adrian Simmons and Richard Engelen have made D-FIRE in MACC happen at all and ensured compatibility within MACC and with the ECMWF production system.

References

M.O. Andreae and P. Merlet. Emission of trace gases and aerosols from biomass burning. *Global Biogeochemical Cycles*, 15(4):955–966, 2001.

L. Giglio. Characterization of the tropical diurnal fire cycle using VIRS and MODIS observations. *RSE*, 108 (4):407–421, 2007.

C. Ichoku, YJ Kaufman, S. Syst, A. Inc, and MD Lanham. A method to derive smoke emission rates from MODIS fire radiative energy measurements. *IEEE TGRS*, 43(11):2636–2649, 2005.

J.W. Kaiser, O. Boucher, M. Doutriaux-Boucher, J. Flemming, Y.M. GOVAERTS, J. Gulliver, A. Heil, L. Jones, A. Lattanzio, J.-J. Morcrette, M.R. Perrone, M. Razinger, G. Roberts, M.G. Schultz, A.J. Simmons, M. Suttie, and M.J. WOOSTER. Smoke in the air. *ECMWF Newsletter*, 119:9–15, Spring 2009a.

J.W. Kaiser, M. Suttie, J. Flemming, J.-J. Morcrette, O. Boucher, and M.G. Schultz. Global Real-time Fire Emission Estimates Based on Space-borne Fire Radiative Power Observations. In *AIP Conference Proceedings*, volume 1100, pages 645–648, 2009b.

J.S. Reid, E.J. Hyer, E.M. Prins, D.L. Westphal, J. Zhang, J. Wang, S.A. Christopher, C.A. Curtis, C.C. Schmidt, D.P. Eleuterio, K.A. Richardson, and J.P. Hoffman. Global monitoring and forecasting of biomass-burning smoke: Description of and lessons from the fore locationg and modeling of buning emissions (FLAMBE) program. *IEEE JSTARS*, 34, 2009.

G.J. Roberts and M.J. Wooster. Fire detection and fire characterization over africa using Meteosat SEVIRI. *IEEE TGRS*, 46(4 Part 2):1200–1218, 2008.

W. Seiler and P.J. Crutzen. Estimates of gross and net fluxes of carbon between the biosphere and the atmosphere from biomass burning. *Climatic Change*, 2(3):207–247, 1980.

G.R. van der Werf, J.T. Randerson, L. Giglio, G.J. Collatz, and P.S. Kasibhatla. Interannual variability in global biomass burning emissions from 1997 to 2004. *ACP*, 6(11):3423–3441, 2006.

M.J. Wooster, B. Zhukov, and D. Oertel. Fire radiative energy for quantitative study of biomass burning: derivation from the bird experimental satellite and comparison to modis fire products. *RSE*, 86(1):83–107, 2003.

M.J. Wooster, G. Roberts, G.L.W. Perry, and Y.J. Kaufman. Retrieval of biomass combustion rates and totals from fire radiative power observations: FRP derivation and calibration relationships between biomass consumption and fire radiative energy release. *JGR*, 110, 2005.

X. Zhang and S. Kondragunta. Temporal and spatial variability in biomass burned areas across the USA derived from the GOES fire product. *RSE*, 2008.

A RetrieveFireEmission.sh

```
#!/bin/ksh
# RetrieveFireEmissions.sh
# Example script for retrieving the real time observed open fire emission fields
# that are generated by the D-FIRE sub-project of the MACC project, see
# http://gems.ecmwf.int . It should be executed on C1A or ECGATE.
# 20090715 j.kaiser@ecmwf.int
set -ex

# (0) setup
# mydate must be in the past and after September 2008.
# list of parameters at http://www.ecmwf.int/services/archive/d/parameters/table=210
# currently valid myparam range: (80-82,87,88,90-92,102).210
mydate=20090713
myparam=81.210 # carbon monoxide

# (1) retrieve 0.1 deg lat-lon daily average CO emission field from MARS
# Units: kg/m2/s
# To retrieve hourly fields instead of the daily ones use:
#   time=0030/'to'/2359/'by'/0100,
rm -f GlobalHiRes.grb
mars <<EOF
  retrieve,
    param=$myparam,
    date=$mydate,
    time=1200,
    step=0,
    area=g,
    target=GlobalHiRes.grb,
    expv=f7i2,
    class=rd,
    type=fc,
    levtype=sfc,
    expect=any
EOF

# (2) take mitigating action if MARS retrieval has failed
if [ ! -s GlobalHiRes.grb ]
then
  print "ERROR in RetrieveFireEmission.sh"
  exit 1
fi

# (3) extract European emission, maintaining the resolution
# area definition: North/West/South/East (deg)
# valid longitude range: [-180,+180]
mars -n <<EOF
  read,
    source=GlobalHiRes.grb,
    area=75/-20/10/60,
    target=EuropeHiRes.grb
EOF
# some diagnostics (average and max value need not be preserved)
grib_ls GlobalHiRes.grb EuropeHiRes.grb
grib_ls -p param,date,time,min,average,max GlobalHiRes.grb EuropeHiRes.grb
gzip -v1f EuropeHiRes.grb

# (4) interpolate global field to T159 reduced Gaussion resolution
```

```
# "-y f" switches flux conservation on
# "-b 1" writes a budget check to stdout and fort.33
export IFS_CYCLE=35r2
%els~nak/bin/firepolate090706 -y f -r 80 -g r -i GlobalHiRes.grb -o GlobalLoRes.grb
~nak/bin/firepolate090820 -y f -r 80 -g r -i GlobalHiRes.grb -o GlobalLoRes.grb
# some diagnostics (average and max value need not be preserved)
grib_ls GlobalHiRes.grb GlobalLoRes.grb
grib_ls -p param,date,time,min,average,max GlobalHiRes.grb GlobalLoRes.grb
gzip -v1f GlobalLoRes.grb

# (5) clean up
rm GlobalHiRes.grb

%els# (6) Note: how to make firepolate090706, which is a version of interpo
# (6) Note: how to make firepolate090820, which is a version of interpo
# provided by Nils Wedi on C1A and ECGATE:
%els# xlf90 -qfree=F90 -qsuffix=cpp=F90 -c ~nak/wrk/NRTfire/firepolate090706.F90 \
# xlf90 -qfree=F90 -qsuffix=cpp=F90 -c ~nak/wrk/NRTfire/firepolate090820.F90 \
# -qextname -q64=largetype -g -O3 -qnohot -qstrict -qsource
%els# xlf90 -o firepolate090706 firepolate090706.o -L /usr/local/lib/eclib/2008/LP64 \
# xlf90 -o firepolate090820 firepolate090820.o -L /usr/local/lib/eclib/2008/LP64 \
#   -l ec.R64.D64.I32 -L/usr/local/lib/metaps/lib/000320 -lemos.R64.D64.I32
# Further optimisation on C1A is possible with -qarch=pwr6 .
```